Integrated luminescent lifetime system for continuous oxygen monitoring

Integrated luminescent lifetime system for continuous oxygen monitoring

Pablo G. Ledesma Lopez, Andreas Tsiamis, Srinjoy Mitra
School of Engineering, Institute for Micro and Nano Systems, The University of Edinburgh
Scottish Microelectronics Centre, Edinburgh, Scotland
pablo.ledesma@ed.ac.uk, a.tsiamis@ed.ac.uk, srinjoy.mitra@ed.ac.uk

***Abstract*—This study proposes a fully integrated optical sensing platform based on photoluminescence lifetime measurements, for continuous monitoring of tissue oxygen levels. The platform incorporates silicon light-emitting diodes (SiLEDs), single-photon avalanche diodes (SPADs), and a functionalized phosphorescence layer using platinum octa-ethyl porphyrin (PtOEP). This paper details the characterization of SiLEDs, improvements in the data acquisition system for enhanced time resolution, and the experimental procedure for oxygen detection. The results demonstrate the sensor's sensitivity to oxygen concentrations, particularly below 20%. Stern-Volmer analysis confirms the platform's linearity and sensitivity to oxygen with an R-squared of 0.9330, making it a promising tool for monitoring oxygenation in diverse microenvironments, including tumorous tissues.**

Keywords—Implantable oxygen sensor, SiLED, SPAD, Phosphorescence Lifetime, PtOEP. *(keywords)*

I. Introduction

Hypoxia is the condition where a group of cells is depleted of oxygen due to the absence of blood supply. Tissue oxygen deficiency (hypoxia) and impaired utilisation of oxygen (dysoxia) are frequent and dangerous conditions generally derived from various emergencies such as trauma, respiratory distress and fainting, and up to more severe ailments like heart failure, stroke, and especially cancer where insufficient blood supply to the microenvironment is a feature in almost all solid tumours [1]. A miniaturised system capable of detecting different oxygen concentrations in a microenvironment could be key to continuously monitoring cancerous tissue growth and progression within the human body through hypoxia [2].

Common strategies to detect hypoxia include immunolabeling endogenous and exogenous markers, but they do not provide a specific oxygen (O_2) concentration or real-time monitoring. Other technologies like Magnetic Resonance Imaging and Positron Emission Tomography require specialized and costly equipment. Additionally, electrochemical and invasive optical sensors use needle-based electrodes or optical fibre probes to measure hypoxia in solid tumours; however, these approaches can constrict vasculature and affect blood flow [3].

Here, we present a fully integrated optical sensor platform based on photoluminescence lifetime measurements. One of the advantages of using lifetime-based measurement is that it is an intrinsic characteristic of a fluorophore, hence independent of the sensor gain or measurement method. Luminescent lifetime is a versatile method that can be used in various phases such as gas, liquid, solid, or combinations thereof. It applies to a wide range of systems with diverse spatial scopes, from individual molecules to cells and the human body [4]. Lifetime measurements have the advantage of resisting photobleaching as they are not reliant on the intensity of fluorescence but rather the decay rate of the excited state [5]. This method requires a pulsed light source directed to the photoluminescent molecule, which emits photons that can then generate a signal in the detector after being excited. We integrated a Complementary Metal-Oxide-Semiconductor (CMOS) chip [4] into our data acquisition system, and a drop-casted photoluminescent sensing layer to test the whole system as an oxygen sensor, as shown in Fig. 1. An array of closely connected source and detector arrays on a single CMOS chip offers numerous benefits. It simplifies the system by eliminating the need for an external light source while also improving signal-to-noise ratio and enabling multimodal sensing capabilities.

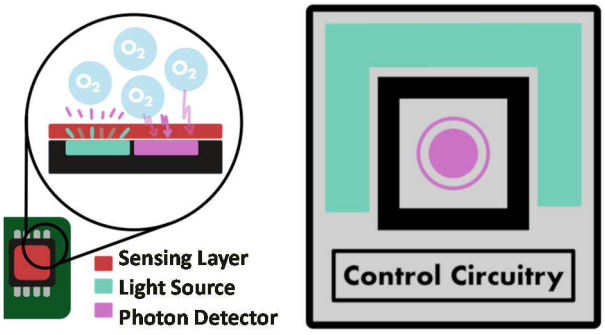

Fig. 1. Diagram of the optical oxygen sensing system and a layout of the luminescent sensor pixel on the chip, composed of SiLEDs as light source and SPADs as a photon detector.

II. Monolithic Integration of Optical Sensing

A. Silicon Light Source and Single Photon Avalanche Detectors

Light from silicon occurs when the current passing through the silicon diode causes electrons and holes to be injected into the silicon crystal. These electrons and holes then recombine, releasing energy in the form of light [6]. Silicon light-emitting diodes (SiLED) have some advantages over traditional LEDs such as compatibility with silicon-based electronic devices. Furthermore, they are tightly integrated into standard fabrication processes and can be placed closer to the detector. This tight integration can be an advantage to further miniaturisation for implantable applications. However, SiLEDs are recognized for their notable low efficiency attributed to their indirect bandgap structure. Nonetheless, this drawback can be disregarded given the intermittent nature of the application.

Single photon Avalanche Diodes (SPADs) are semiconductor devices that detect single photons of light and convert them into electrical signals, which electronic circuits can then amplify and process. They are susceptible to dark counts, which are false positive signals produced by thermal and quantum mechanical effects. SPADs, on the other hand, can detect single photons with an efficiency of up to 45% [7]. SPADs have several advantages over other types of light sensors. They have a high sensitivity to single photons, making them well-suited for applications with low light levels. They also have a fast response time and can operate at high

speeds, which makes them useful for time-resolved measurements.

SiLEDs and SPADs can be fabricated together using commercially available CMOS technology, avoiding the need for additional chip processing. This allows easy integration of readout circuitry and instrumentation into a single device. Moreover, the ability to place them in a close distance between the two also raises the likelihood of detecting any emitted photons. In addition to the small footprint, which is paramount for an implantable device. However, an appropriate phosphorescent coating (the sensing layer) has to be added to functionalise the chip for a particular gaseous specimen.

B. Functionalised Phosphorescence Layer

Room-temperature phosphorescent organic materials have gained interest due to their unique optical and electronic properties, such as long emission lifetime, afterglow, large Stokes shifts, and abundant triplet states. These attributes make them well-suited for sensing applications aimed at detecting and measuring specific analytes [8]. The materials could potentially revolutionise sensor technology by providing better sensitivity, selectivity, and stability. Phosphorescence sensors have a key advantage in their ability to remove interference from short-lifetime background fluorescence and scattering light [9]. Time-resolved luminescence technology effectively reduces the impact of interfering factors, leading to accurate and reliable sensor measurements. The delayed luminescence phenomenon exhibited by phosphorescent materials allows for precise detection. Phosphorescent materials such as Platinum Octa-ethyl Porphyrin (PtOEP) sensing films integrated with silicon light-emitting diodes and single-photon avalanche diodes greatly enhance the performance of oxygen sensors due to their susceptibility to luminescence quenching by oxygen, making them ideal for optical oxygen sensors [10]. Phosphorescent dye-based optical oxygen sensors are widely used in industry and academia due to their high accuracy, simple instrumentation, and wide range of applications [11].

III. Experiments and Discussion

A. SiLED Characterisation

In order to define suitable fluorophores that can be functionalised with the current integrated circuit, a characterisation of the SiLED must be performed. Characterising the SiLED involves measuring its emission spectrum as the principal operational parameter. The emission spectrum of the SiLED can reveal the range of wavelengths it can emit and thus help identify potential fluorophores that can be excited by it.

To obtain the spectrum, a 1500 µm diameter, 0.50 NA optical fibre probe was positioned near the SiLED to collect the emitted light with a Spectrometer (Thorlabs CCS200/M). The emission spectrum of the SiLED was found to be centred at a wavelength of 680 nm with a low limit emission at around 450 nm and a high limit emission at around 950 nm, as reported in Fig. 2, the emission spectrum closely resembles those presented in previous literature [12]. This information is crucial for selecting fluorophores with absorption spectra matching the emission spectrum of the SiLED.

Platinum octa-ethyl porphyrin (PtOEP) was selected as it can absorb light up to 536 nm, which falls within the emission spectrum of the SiLED, and its ability to be quenched by oxygen, hence commonly used in sensing applications.

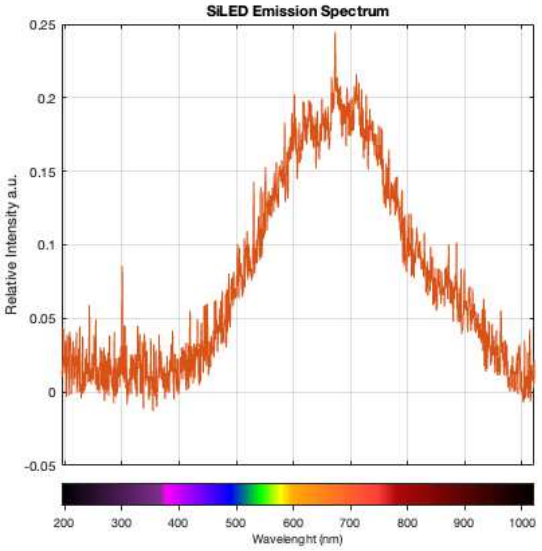

Fig. 2. Emission Spectrum of the Sillicon LED (SiLED) present in the photoluminesce sensing platform.

B. Data Acquisition System

Accurately measuring and analysing events that occur on nanosecond or microsecond timescales is of utmost importance in scientific research and technological applications. This is especially critical in fields like molecular dynamics, biological studies, and time-resolved spectroscopy. To address this need, there is a growing demand for event-based data acquisition systems with a higher time resolution, enabling researchers to capture and analyse events with greater precision and detail. We developed a data acquisition system with bin size down to a nano-second level.

By doing so, we can achieve a significantly higher level of temporal accuracy and resolution, enabling us to observe and study processes that were previously inaccessible. To enhance the efficiency and speed of processing photon timing measurements, a time correlation single photon counting (TCSPC) algorithm was developed specifically for an ARM Cortex-M7 Microcontroller (MCU) operating at 600 MHz. The system includes high-speed digital signal level shifters to enable the MCU 3.3V Low Voltage Transistor-transistor Logic (LVTTL) to send and receive data from the 5V Transistor-transistor Logic (TTL) sensing chip. A custom power supply that provides the high voltage required to power the SPADs and generation of SiLED pulses and a USB-C connection for communication and power is integrated into a custom Printed Circuit Board (PCB). Each pixel output is connected to a shared Data line via a multiplexer, SPAD pulses are transformed into digital signals and buffered through an inverter chain. During periods of inactivity, they are isolated from the Data line using a transmission gate. The Data Output from the chip is connected to the level shifter and then to a General-Purpose Digital Input in the MCU, while the control outputs to enable pixel selection go from the MCU to the sensing chip. These

enhancements enable accurate capture and processing of photon arrival times with nanosecond precision.

To verify the system's time resolution capabilities, experiments were carried out in a lightproof enclosure using an Arbitrary Function Generator acts as a pulse generator to control the SiLED light source, as there is no driver circuitry on the chip. The signal consisted of a 30-nanosecond pulse with an 8.6 ns rise and fall time, while the SPAD window remained open for 1000 nanoseconds, as depicted in Fig. 3.

The results of the experiment showed a temporal accuracy of seven nanoseconds per bin for the data acquisition system; this provides the required time resolution for potential multiple analytes with phosphorescence lifetimes in the region of tens of nanoseconds up to seconds.

Examples of such analytes include pH (lifetime between 8 to 18 ns [13], [14]), Hydrogen Sulfide (lifetime in the region of 169 to 745 ns), and Nitric Oxide (between 50 to 230 ns, depending on the system [15]). All of these gases are known to play a role in mediating the tumour microenvironment [16].

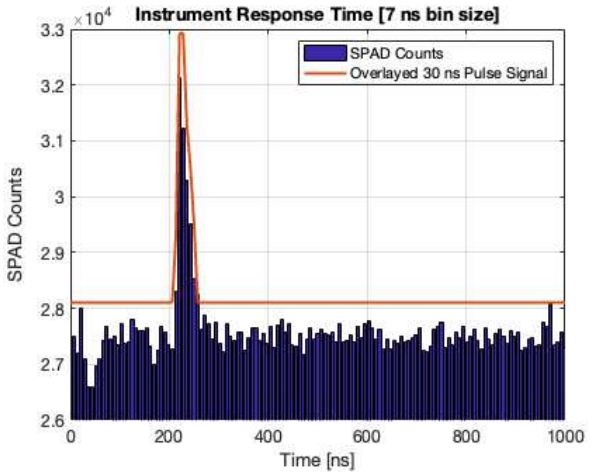

Fig. 3. Instrument response time of the TCSP system with the overlayed 30 ns pulsed signal used for characterisation.

C. *Gaseous Oxygen Measurements*

A gas test was performed as a proof of concept for the system, where Polystyrene (PS, average MW 280,000, GPC grade) was used as an encapsulation matrix for the fluorophore. Platinum octa-ethyl porphyrin (PtOEP) was used as a phosphorescent dye, in addition to toluene as a solvent. all of these were purchased from Sigma Aldrich (www.sigmaaldrich.com). A PtOEP-PS solution was prepared by dissolving 100 mg of PS and 10 mg of PtOEP in toluene, then stirred for 15 minutes until dissolved and mixed to form a 1:10 w/w ratio of PtOEP-PS. With a pipette, 50 µl of the solution was drop-cast on top of the sensing area of a previously wire-bonded chip. The chip was then left in a dark environment at room temperature to ensure the evaporation of the remaining solvent.

The packaged chip comprised of an 8x8 SiLED-SPAD pixel array (Fig.4) provided by Guerrero et al. [17], was then tested in a dedicated custom oxygen station as depicted in Fig. 5. The main sensor with its daughter PCB and micro-controller was placed in a fully obscured airtight box, which provided a controlled gaseous environment. The gaseous content of the box can be replaced with Oxygen, Nitrogen or a mixture of both. A commercially available oxygen sensor with an alkaline electrode sensing element and meter (Greisinger GOX 100T) was used as control. Light source pulse generation and SPAD count readout were obtained with the use of the previously mentioned custom PCB, which sends the pulse counts to the PC for graphical representation.

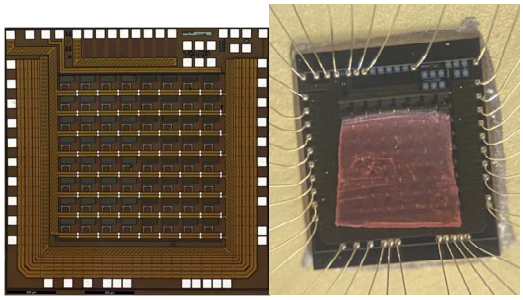

Fig. 4. Micrograph of the CMOS chip with a 64-pixel sensor array with integrated excitation and detection, and a photograph of the wirebonded sensor with a sensing layer placed on top.

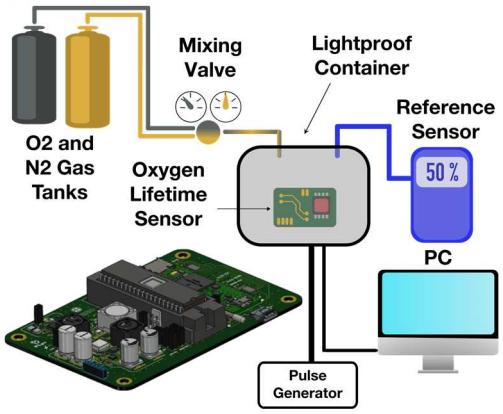

Fig. 5. Experimental setup layout and PCB 3D Model. The sensor, PCB and reference sensor are inside a lightproof container flooded with gas that replicates different oxygen concentrations. Excitation pulses are generated externally with a pulse generator.

In order to obtain lifetimes, the chamber was flushed for 2 minutes with the desired oxygen gas concentration. The permeated gas is constant over the entire measurement. The sensor is excited with a 50 µs pulse from the correspondent pixel SiLED with 30 mA current. Afterwards, the matching SPAD is exposed, and the pixel is allowed to discharge from, before the next excitation period.

Each cycle count is recorded sequentially into 400 equal user-defined bins with a 500 nanosecond time resolution for a specified number of cycles; each bin is used to reconstruct a histogram of photon detection and time. The data is sent to a PC to be represented graphically (Fig.6), before being processed. The data is then fitted to a fluorescence decay model according to equation (1) [18]. Where I is the intensity of the signal, Io is the intensity at time zero (upon excitation), τ is the lifetime, and C is the number of dark counts of the SPAD. The sensor was tested at different oxygen concentrations ranging from 0 to 75% to demonstrate a system response and linearity.

$$I(t) = I_0 e^{-(t/\tau)} + C \quad (1)$$

A control sensor was used to confirm concentration accuracy. 20,000 excitation cycles of 550 µs each over approximately 12 seconds per pixel and 12 minutes for the entire 64-pixel array were performed under constant oxygen concentration. For each of the remaining measurements, the same procedure was followed.

In the raw SPAD count data acquired (Fig. 6), a difference in the signal between concentrations is perceptible. The photoluminescence response is stronger when lower concentrations of oxygen are present. In contrast, the phosphorescent strength of PtOEP in the polymer diminishes as the level of oxygen increases [19]. However, the proposed application does not need to be accurate at higher concentrations as O_2 measurements in hypoxic environments are in low values, in the region of 0.3% up to 7% (e.g., average oxygen concentration for healthy breast tissue is 6.8% and tumorous tissue is 1.3% [20]). Since the luminescence is not being quenched there is a stronger signal at the required low oxygen values.

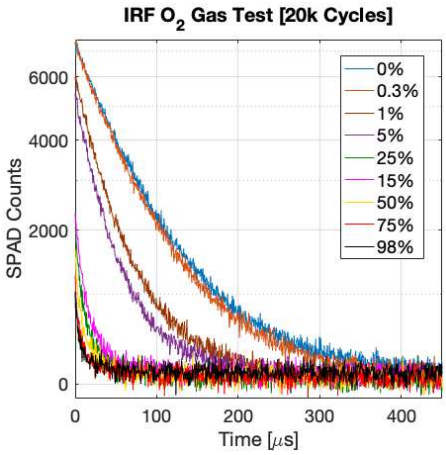

Fig. 6. Comparison of extracted data from a single pixel with a cycle count of 10,000, at different oxygen concentrations. Each cycle has a SPAD window of 500 µs after a 50 µs excitation pulse, the SPAD is activated after the light pulse to avoid any light detection not related to the phosphorescent effect.

The data were curve-fitted to the exponential decay model shown in equation (1), and the lifetime values obtained were used to characterise the sensor with the standard approach using Stern-Volmer analysis as in equation (2).

$$\frac{I_0}{I} = \frac{\tau_0}{\tau} = 1 + K_{sv} \cdot [Q] \quad (2)$$

Where τ_0 and τ are the lifetimes in the absence and presence of oxygen, [Q] being the correspondent analyte concentration and K_{sv} the extracted Stern-Volmer constant from the fit, which quantifies quenching efficiency and how sensible is the sensor to the analyte. The sensor results are presented in a Stern-Volmer plot as shown in Fig. 7. The error bars represent the standard deviation between lifetimes obtained from sixteen randomly selected pixels. The sensor shows a linear response across the measured concentrations, with better sensitivity to oxygen in concentrations lower than room atmosphere (21%) above this the lifetimes are very close together so it is more difficult to differentiate the signals as can be seen in Fig. 6.

When compared with the ideal linearity fit the results showed a high R-squared number implying that Stern-Volmer analysis fits well with the data acquired. Most notably the lifetime measured at 0% oxygen atmosphere was 84.81 µs which is consistent with the literature showing those lifetimes for PtOEP-PS layers [21].

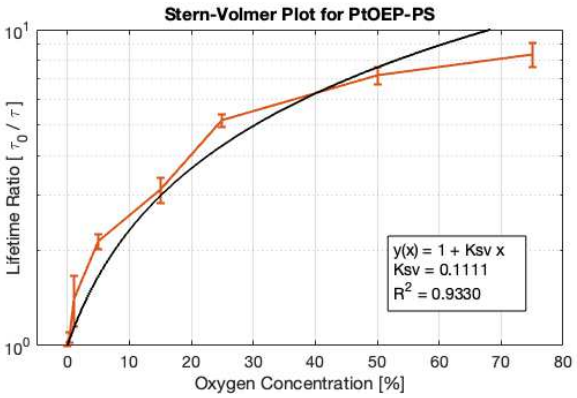

Fig. 7. Stern-Volmer responses of PtOEP-PS sensor at different concentrations of gaseous oxygen at room temperature. Orange line represents the data obtained experimentally, while the blue line shows the ideal linearity fit for the sensor.

The results also represent a clear difference in the obtained lifetimes across different oxygen concentrations, the acquired data suggest that the sensor is highly sensitive to oxygen especially when the concentration is below normal atmospheric conditions. The results indicate a small difference at higher concentrations, but the obtained lifetimes are so similar that they can be easily misinterpreted.

Some reasons for not having a perfect fit could be due to the use of weak and broad wavelength light sources as in the SiLEDs. Hence, the PtOEP film is not excited in its peak absorption wavelength, emitting much fewer photons, especially when high values of oxygen are present. As sixteen random SPADS were selected, and not characterised extensively, some pixels can suffer a larger than average dark count rate, which added noise to the data [22].

Despite that, the system can be compared head-to-head with the four most common phosphorescence lifetime platforms operating in the time domain. An adapted Table I from R Sen et al. [23] shows a summary of the main features of the four platforms compared with our work. The integrated light source/detector combo enables our system to be smaller, and our custom algorithm enhances the lifetime detection range and a large number of data points which are easier to fit.

IV. CONCLUSION

This work demonstrated the integration route of various technologies including SiLEDs, SPADs, and phosphorescent dye-based layers and their potential as a platform for generalised photoluminescent sensing. We have shown that the platform can detect lifetimes in the region of tens of nanoseconds which can target multiple analytes apart from oxygen such as hydrogen sulfide, nitric oxide, and pH. To demonstrate the effectiveness of the platform a gas test was performed for oxygen concentration.

TABLE I. COMPARISON OF DIFFERENT PHOSPHORESCENCE LIFETIME MEASUREMENT PLATFORMS.

System/Parameter	Victor TRF Reader [24]	Cary Eclipse Spectrometer [25]	TPX3 PLIM Imager [26]	Becker&Hickl PLIM Imager [27]	**Nymph One µS (This work)**
Measurement Method	Rapid Lifetime Determination	Phosphorescence Decay / Binnig	TCSPC	Multi-channel Scaler	TCSPC
Excitation Source	External 15W Flashlamp	External 75 W Flashlamp	External LED, 40 mW	External Laser, 10 mW	Integrated SiLED 50 nW
Excitation Wavelength	340 ± 60 nm (filter)	390 ± 10 nm (grating)	390 nm	405 nm	550 nm
Detector Type	PMT	PMT	Time-stamping Camera	PMT	SPAD
No of points on decay (time bins)	2	10-20	1024	1024	100-30,000
Decay Fitting	Pseudo 1-exponential	1/2-exponential	1/2-exponential	1/2-exponential	1/2-exponential
Measured LT range	>10 µs	>10 µs	>100 ns	>100 ns	>30 ns
Price Range	>$30k	>$30k	>$60k	>$400k	< $5k
Size (LxWxH mm)	500 x 200 x 270 mm	644 x 608 x 271 mm	525 x 375 x 300 mm	NA	130 x 80 x 30 mm

The extracted lifetimes for this test using a PtOEP-PS luminescent layer with a 0% oxygen concentration was ~85 µs which adheres to previously reported literature. The measurements were made at different concentrations and crucially showed the oxygen-dependent quenching of photoluminescence, in addition, the Stern-Volmer plot indicates a more sensitive device across lower oxygen concentrations crucial for measuring how oxygenation impacts healthy and tumorous tissue [20]. Further work is being done to integrate the luminescent layer directly over the chip for oxygen sensing and test the system for reversibility, as well as the pulse generation towards a miniaturised embedded system and its potential application for monitoring the tumorous microenvironment and the effectiveness for better understanding of therapies.

ACKNOWLEDGMENT

This work was supported by the National Council of Science and Technology (CONACyT), Grant Number 2019-000021-01EXTF-00684. The authors thank Ricardo Jose Sta Maria Guerrero and Alan Murray for providing the IC and Edoardo Charbon for providing the SPAD design. For the purpose of open access, the author has applied a Creative Commons Attribution(CC BY) license to any author accepted manuscript version arising from this submission.

REFERENCES

[1] X. Jing *et al.*, 'Role of hypoxia in cancer therapy by regulating the tumor microenvironment', *Mol. Cancer*, vol. 18, no. 1, p. 157, Dec. 2019, doi: 10.1186/s12943-019-1089-9.

[2] V. Petrova, M. Annicchiarico-Petruzzelli, G. Melino, and I. Amelio, 'The hypoxic tumour microenvironment', *Oncogenesis*, vol. 7, no. 1, p. 10, Jan. 2018, doi: 10.1038/s41389-017-0011-9.

[3] I. Godet, S. Doctorman, F. Wu, and D. M. Gilkes, 'Detection of Hypoxia in Cancer Models: Significance, Challenges, and Advances', *Cells*, vol. 11, no. 4, p. 686, Feb. 2022, doi: 10.3390/cells11040686.

[4] M. Y. Berezin and S. Achilefu, 'Fluorescence Lifetime Measurements and Biological Imaging', *Chem. Rev.*, vol. 110, no. 5, pp. 2641–2684, May 2010, doi: 10.1021/cr900343z.

[5] F. Fang, D. Zhao, Y. Zhang, M. Li, J. Ye, and J. Zhang, 'Europium-Doped Nanoparticles for Cellular Luminescence Lifetime Imaging *via* Multiple Manipulations of Aggregation State', *ACS Appl. Bio Mater.*, vol. 3, no. 8, pp. 5103–5110, Aug. 2020, doi: 10.1021/acsabm.0c00580.

[6] P. M. Fauchet, 'Practical Nanoscale Silicon Light Emitters', *MRS Online Proc. Libr. OPL*, vol. 486, pp. 21-undefined, 1997, doi: 10.1557/PROC-486-21.

[7] K. Morimoto and E. Charbon, 'A Scaling Law for SPAD Pixel Miniaturization', 2021.

[8] Y. Sun *et al.*, 'Purely Organic Blue Room-Temperature Phosphorescence Activated by Acrylamide In Situ Photopolymerization', 2022.

[9] M. Xin *et al.*, 'A class of fascinating optoelectronic materials: Triarylboron compounds', 2010.

[10] 'Intersystem Crossing Mechanisms in the Room Temperature Phosphorescence of Crystalline Organic Compounds', *Bull Chem Soc Jpn*, 2018.

[11] K. Koren, 'Tuning the dynamic range and sensitivity of optical oxygen-sensors by employing differently substituted polystyrene-derivatives', 2013.

[12] A. F. Bulling and P. J. Venter, 'Improved light extraction efficiency of complementary metal-oxide semiconductor hot carrier lights sources with the use of improved back-end-of-line light directing structures', *Opt. Eng.*, vol. 58, no. 06, p. 1, Jun. 2019, doi: 10.1117/1.OE.58.6.065105.

[13] P. J. Pacheco-Liñán, I. Bravo, M. L. Nueda, J. Albaladejo, and A. Garzón-Ruiz, 'Functionalized CdSe/ZnS Quantum Dots for Intracellular pH Measurements by Fluorescence Lifetime Imaging Microscopy', *ACS Sens.*, vol. 5, no. 7, pp. 2106–2117, Jul. 2020, doi: 10.1021/acssensors.0c00719.

[14] J. R. Shakirova *et al.*, 'Intracellular pH Sensor Based on Heteroleptic Bis-Cyclometalated Iridium(III) Complex Embedded into Block-Copolymer Nanospecies: Application in Phosphorescence Lifetime Imaging Microscopy', *Adv. Funct. Mater.*, vol. 33, no. 10, p. 2212390, Mar. 2023, doi: 10.1002/adfm.202212390.

[15] A. Denicola, J. M. Souza, R. Radi, and E. Lissi, 'Nitric Oxide Diffusion in Membranes Determined by Fluorescence Quenching', *Arch. Biochem. Biophys.*, vol. 328, no. 1, pp. 208–212, Apr. 1996, doi: 10.1006/abbi.1996.0162.

[16] C. Szabo, 'Gasotransmitters in cancer: from pathophysiology to experimental therapy', *Nat. Rev. Drug Discov.*, vol. 15, no. 3, pp. 185–203, Mar. 2016, doi: 10.1038/nrd.2015.1.

[17] R. J. S. M. Guerrero, A. Murray, and E. Charbon, 'Photoluminescence Lifetime Sensor Pixels using SPADs and Silicon LEDs in Commercial CMOS', in *2019 IEEE SENSORS*, Montreal, QC, Canada: IEEE, Oct. 2019, pp. 1–4. doi: 10.1109/SENSORS43011.2019.8956921.

[18] R. K. Henderson, B. R. Rae, and D.-U. Li, 'CMOS sensors for fluorescence lifetime imaging', in *High Performance Silicon Imaging*, Elsevier, 2020, pp. 377–412. doi: 10.1016/B978-0-08-102434-8.00012-X.

[19] R. N. Gillanders, M. C. Tedford, P. J. Crilly, and R. T. Bailey, 'Thin film dissolved oxygen sensor based on platinum octaethylporphyrin encapsulated in an elastic fluorinated polymer', *Anal. Chim. Acta*, vol. 502, no. 1, pp. 1–6, Jan. 2004, doi: 10.1016/j.aca.2003.09.053.

[20] S. R. McKeown, 'Defining normoxia, physoxia and hypoxia in tumours—implications for treatment response', *Br. J. Radiol.*, vol. 87, no. 1035, p. 20130676, Mar. 2014, doi: 10.1259/bjr.20130676.

[21] K. Koren, S. M. Borisov, R. Saf, and I. Klimant, 'Strongly Phosphorescent Iridium(III)-Porphyrins - New Oxygen Indicators with Tuneable Photophysical Properties and Functionalities', *Eur. J. Inorg. Chem.*, vol. 2011, no. 10, pp. 1531–1534, Apr. 2011, doi: 10.1002/ejic.201100089.

[22] P. W. R. Connolly, X. Ren, R. K. Henderson, and G. S. Buller, 'Hot pixel classification of single-photon avalanche diode detector arrays using a log-normal statistical distribution', *Electron. Lett.*, vol. 55, no. 18, pp. 1004–1006, Sep. 2019, doi: 10.1049/el.2019.1427.

[23] R. Sen, L. Li, A. V. Zhdanov, R. D. L. Gaspar, and D. B. Papkovsky, 'Phosphorescence lifetime measurements with sensor materials: Comparison of the four different detection platforms', *Sens. Actuators B Chem.*, vol. 371, p. 132496, Nov. 2022, doi: 10.1016/j.snb.2022.132496.

[24] PerkinElmer, 'VICTOR Nivo Multimode Microplate Reader', Revvity. Accessed: Mar. 01, 2024. [Online]. Available: https://www.revvity.com/gb-en/Product/victor-nivo-advanced-f-abs-filter-lu-hh35000500

[25] 'Fluorescence Spectrometer, Fluorometer, Cary Eclipse | Agilent'. Accessed: Mar. 01, 2024. [Online]. Available: https://www.agilent.com/en/product/molecular-spectroscopy/fluorescence-spectroscopy/fluorescence-systems/cary-eclipse-fluorescence-spectrophotometer

[26] R. Sen *et al.*, 'New luminescence lifetime macro-imager based on a Tpx3Cam optical camera', *Biomed. Opt. Express*, vol. 11, no. 1, p. 77, Jan. 2020, doi: 10.1364/BOE.11.000077.

[27] 'DCS-120 Confocal FLIM System', Becker & Hickl GmbH. Accessed: Mar. 01, 2024. [Online]. Available: https://www.becker-hickl.com/products/confocal-flim-system/